International Journal of Nanomedicine

Dovepress
open access to scientific and medical research

Open Access Full Text Article

ORIGINAL RESEARCH

Zirconium Oxide Thin Films Obtained by Atomic Layer Deposition Technology Abolish the Anti-Osteogenic Effect Resulting from miR-21 Inhibition in the Pre-Osteoblastic MC3T3 Cell Line

This article was published in the following Dove Press journal:
International Journal of Nanomedicine

Aleksandra Seweryn[1]
Ariadna Pielok[2]
Krystyna Lawniczak-Jablonska[1]
Rafal Pietruszka[1]
Klaudia Marcinkowska[2]
Mateusz Sikora[2]
Bartlomiej S Witkowski[1]
Marek Godlewski[1]
Krzysztof Marycz[2,3]
Agnieszka Smieszek[2]

[1]Institute of Physics, Polish Academy of Sciences, Warsaw PL-02668, Poland; [2]Wroclaw University of Environmental and Life Sciences, Department of Experimental Biology, Wroclaw PL-50375, Poland; [3]Cardinal Stefan Wyszynski University, Collegium Medicum, Warsaw PL-01938, Poland

Correspondence: Aleksandra Seweryn
Polish Academy of Sciences, Aleja Lotnikow 32/46, Warsaw PL-02668, Poland
Tel +48 22 116 33 99
Fax +48 22 843 09 26
Email aseweryn@ifpan.edu.pl

Agnieszka Smieszek
Wroclaw University of Environmental and Life Sciences, Norwida St. 27 B, Wroclaw PL-50-375, Poland
Tel +48 71 320 5229
Fax +48 22 843 09 26
Email agnieszka.smieszek@upwr.edu.pl

Introduction: The development of the field of biomaterials engineering is rapid. Various bioactive coatings are created to improve the biocompatibility of substrates used for bone regeneration, which includes formulation of thin zirconia coatings with pro-osteogenic properties. The aim of this study was to assess the biological properties of ZrO_2 thin films grown by Atomic Layer Deposition (ALD) technology (ZrO_2^{ALD}).

Methodology: The cytocompatibility of the obtained layers was analysed using the mice pre-osteoblastic cell line (MC3T3) characterized by decreased expression of microRNA 21-5p (miR-21-5p) in order to evaluate the potential pro-osteogenic properties of the coatings. The in vitro experiments were designed to determine the effect of ZrO_2^{ALD} coatings on cell morphology (confocal microscope), proliferative activity (cell cycle analysis) and metabolism, reflected by mitochondrial membrane potential (cytometric-based measurement). Additionally, the influence of layers on the expression of genes associated with cell survival and osteogenesis was studied using RT-qPCR. The following genes were investigated: B-cell lymphoma 2 (*Bcl-2*), Bcl-2-associated X protein (*Bax*), *p53* and *p21*, as well as osteogenic markers, i.e. collagen type 1 (*Coll-1*), osteopontin (*Opn*), osteocalcin (*Ocl*) and runt-related transcription factor 2 (*Runx-2*). The levels of microRNA (miRNA/miR) involved in the regulation of osteogenic genes were determined, including miR-7, miR-21, miR-124 and miR-223.

Results: The analysis revealed that the obtained coatings are cytocompatible and may increase the metabolism of pre-osteoblast, which was correlated with increased mitochondrial membrane potential and extensive development of the mitochondrial network. The obtained coatings affected the viability and proliferative status of cells, reducing the population of actively dividing cells. However, in cultures propagated on ZrO_2^{ALD} coatings, the up-regulation of genes essential for bone metabolism was noted.

Discussion: The data obtained indicate that ZrO_2 coatings created using the ALD method may have pro-osteogenic properties and may improve the metabolism of bone precursor cells. Given the above, further development of ZrO_2^{ALD} layers is essential in terms of their potential clinical application in bone regenerative medicine.

Keywords: ALD, zirconia-based coatings, pro-osteogenic properties, cytocompatibility, osteoblasts precursors

Over the years, various methods aimed at improving the healing process of bone tissue have been tested.[1] This is largely due to the fact that bone fractures, even when

attended to properly, need a prolonged period of time to fully heal as the formation of new, functional bone tissue is multi-staged and complicated.[2] Some diseases[3] can further extend the reconvalescence time; therefore, it is a great challenge for regenerative medicine to develop novel methods that would shorten the healing time and ensure better resistance to the recurrence of injury.

The development of nanomaterials/nanocoatings that can positively affect the quality and speed of healing processes perfectly fits this trend. In recent years, zirconium oxide (ZrO_2) materials have become well known due to their biological properties.[4,5] Especially interesting evidence has been published regarding the use of zircon oxide as a coating that could improve the osteointegration of implants.[5] For these reasons, this study is aimed at evaluating the ZrO_2 coatings obtained by Atomic Layer Deposition (ALD)[6] technology. ZrO_2 is a biocompatible material showing effective anti-bacterial activity.[7]

The basis of the ALD method is a sequential introduction of selected chemical compounds into the reaction chamber. Each dose of the precursor is separated by a purge of the growth chamber by an inert gas, e.g. argon or nitrogen.[8] Due to pulse separation, the reaction between reagents occurs only on the substrate. The ALD processes are self-limiting, since deposition is blocked once the surface is saturated with a given precursor. After optimizing the parameters of the process, only the number of ALD cycles has to be estimated to reach a desired film thickness.[9] The obtained films are highly reproducible, and the deposition process depends weakly on the substrate used. Time separation of precursor pulses provides the possibility of using highly reactive chemicals and thus a low deposition temperature. Even at room temperature, deposition of layers is possible.[10] Despite the low temperature of growth, the resulting layers are of high quality and are highly homogeneous.[11] The conformal growth of ALD coatings allows the formation of homogeneous layers on complex surfaces.[12,13] This is a huge advantage of ALD technology for applications in biology and medicine. Another advantage of ALD is the possibility of obtaining biocompatible films. Hydroxyapatite growth by ALD has already been tested and proven to improve the attachment pre-osteoblast (MC3T3 cell line).[14–16]

The bioactivity of implant coating can be guaranteed by low-temperature deposition of films and this can be assured by the application of ALD technology.

For the growth of ZrO_2 coatings by ALD technology, various precursors of zirconium (Zr) were tested, such as tetrakisdimethylamidozirconium ($Zr(NMe_2)_4$), tetrakisethylmethylamidozirconium $Zr(NMeEt)_4$, tetrakisdiethylamidozirconium $Zr(NEt_2)_4$.[6] As an oxidant (oxygen precursor), water vapors,[17] ozone[18] or pure oxygen[19] were reported. The proper selection of process condition is crucial, as the crystallographic phase of the zirconium oxide layers depends on the precursors used and the deposition temperature.[10] It also turned out that the thickness of the layer influences crystallization. Initially, the layer is amorphous; later, with increasing film thickness, it becomes crystalline.[10] Amorphous films form high-quality interfaces between the substrate and the layer. This is of great importance for its toughness and smoothness.[11]

Moreover, there were first reports that zirconium oxide thin films have potential applications in regenerative medicine.[5,20-22] This is because ZrO_2 coatings are cytocompatible with immunocompetent cells like monocytes/macrophages. Together with its antibacterial effect, ZrO_2[7] may prevent peri–implant bone resorption and peri–implant soft inflammation.[23] Moreover, it was previously shown that ZrO_2 coatings may promote adhesion and spreading of progenitor cells and bone-forming cells, i.e. osteoblasts. The ZrO_2 coatings influenced proliferative activity, enhancing both cell division and the formation of a well-organized, firm monolayer of cells. More importantly, ZrO_2 induces the differentiation of multipotent stromal cells. The osteogenic potential of ZrO_2 coatings was confirmed using multipotent cells of mesenchymal origin (MSC) including bone-marrow and adipose tissue-derived stromal cells (BMSC and ASC, respectively). The pro-osteogenic properties of ZrO_2 coatings are reflected by their ability to promote mineralization of extracellular matrix and formation of osteonodules rich in calcium and phosphorous deposits. Bearing in mind the high bioactivity of thin ZrO_2 layers and their positive effect on bone healing confirmed by in vivo studies, these coatings are commonly used to enhance the biocompatibility of various implants.[22]

The biological activity of zirconium oxide coatings can be also improved by conjugation with silicon-based layers. We have previously shown[22] that SiO_2/ZrO_2 coatings exert pro-osteogenic properties and can serve as an ideal carrier for drug delivery.[22] SiO_2/ZrO_2 coatings obtained using the sol-gel technique on stainless steel were functionalized with a popular anti-diabetic drug – metformin. Such hybrid coatings improved the differentiation of ASC and

resulted in the formation of a highly mineralized extracellular matrix.

As we showed above, the biocompatible properties of ZrO_2 are known, but influence of zirconia coatings obtained by the ALD on pre-osteogenic cells has not been yet studied. The technology can influence surface topography and chemical composition of the materials, which have a direct impact on cell behavior. Sensitivity of osteoblasts to very subtle chemical changes of the surface is known.[24] Additionally, the ALD technology allows the deposition of high-quality layer by relatively low temperature (even below 100°C). Low process temperatures may enable the layer deposition on temperature-sensitive materials, which is important for new implant materials such as biopolymers.

Bearing in mind the above reports (i.e. the high bioactivity of ZrO_2 and the great potential of ALD technology) the aim of the present study was to obtain ZrO_2 films as a biomaterial with pro-osteogenic properties. Films deposited by ALD were investigated. In order to test the cytocompatibility of the obtained coatings, in this study we used the well-established MC3T3 model. In order to determine the pro-osteogenic activity of the layers, we used MC3T3 transfected with miR-21 inhibitor ($MC3T3_{inh21}$).

The miR-21-5p molecule is considered to be the key regulator of osteogenic differentiation of progenitor cells. This miRNA was shown to play a crucial role in terms of the regulation of the metabolism of bone-forming and bone-resorbing cells. It was shown that exogenously added miR-21 mimics into BMSC cultures, induces differentiation of osteoblasts and promotes the formation of a functional extracellular matrix, rich in mineralized nodules. This was also associated with an increased expression of mRNA for main early- and late osteogenic markers including alkaline phosphatase (*ALP*), osteocalcin (*OCL*), bone morphogenetic protein 2 (*BMP-2*) and the master regulator of the osteogenesis, i.e. runt-related transcription factor (*RUNX-2*). It was also shown that inhibition of miR-21 had the opposite effect, which resulted in the decreased osteogenic ability of BMSC.[25] Moreover, miR-21 was recognized as a molecule that promotes angiogenesis, crucial for proper bone healing. The angiogenic potential of miR-21 increased the expression of vascular endothelial growth factor (VEGF) and hypoxia-inducible factor-1α (HIF-1α).[26]

The present study was performed for ALD-deposited ZrO_2 films on glass cover slips. We report that such films are highly cytocompatible and we present a physicochemical analysis of such layers deposited onto a silicon substrate. We determined the influence of coatings on cell proliferation, viability and metabolic potential. The studies included analysis of the mRNA and miRNA of osteogenic-related molecules.

Materials and Methods

ALD Growth Method

The layers were obtained using a Savannah-100 Cambridge NanoTech ALD reactor (now Veeco Savannah S100). Tetrakis(dimethylamido)zirconium: TDMA-Zr (CAS number 19756-04-8) and deionized water were used as precursors of metal and oxygen, respectively. High purity nitrogen gas (6N) was used to purge the chamber. With such precursors, ALD growth proceeded according to the double exchange reaction:[19]

$$Zr\left[(CH_3)_2N\right]_4 + 2H_2O \rightarrow ZrO_2 + 4HN(CH_3)_2$$

Before the process, the reaction chamber and the zirconium precursor were preheated to 100° and 65° C, respectively. Constant temperature was maintained throughout the process. The reactor chamber was under controlled vacuum (below 66 Pa). The process was carried out in cycles. One cycle consisted of a metal precursor pulse, a purge pulse, an oxygen precursor pulse and a purge pulse. The pulse length of the precursors was selected to be 0.04 s for water and 0.2 s for TDMA-Zr. The purge time after metal and oxygen precursor pulses was 10 s. Additionally, after each precursor dose, a 3 s waiting phase was applied. The growth rate by such established times was estimated to be 1.9 Å/cycle.

Substrate

The layers used for physical investigations were grown on a silicon wafer (100), which was cut into 1 cm x 1 cm pieces. Layers used for bio experiments were deposited on cover slips with a diameter of 13 mm. In order to eliminate any contaminants that could affect the adhesion of the layer to the substrate or its homogeneity, the substrates were washed three times for 5 min, using an ultrasonic cleaner at 37°C. The first bath was carried out in isopropanol and the following two in deionized water. After the completed purification process, all substrates were dried in a high purity nitrogen (5N) stream and then placed in the growth chamber of the ALD reactor.

Test Equipment

A NanoCalc 2000-UV/VIS Mikropack (GmbH) spectrometer with software was used to determine the thicknesses

of the resulting coatings. Measurements of surface morphology and thicknesses distribution were made using a Hitachi SU 70 Scanning Electron Microscope (SEM) with 1.5-nm resolution capacity. A secondary electron detector and an electron-accelerating voltage of 15 kV were used. Top-view and cross-section (CS) images were obtained. To determine the quality of the surface and interface of the considered ZrO_2 layer, X-ray reflectometry (XRR) analysis was made. A Panalytical X'Pert Pro MRD diffractometer equipped with an X-ray tube generating radiation with a wavelength 1.54056 Å, hybrid two-bounce Ge (220) monochromator and Pixel detector was used. In front of the detector, a Parallel Plate Collimator with 0.4 rad Soller slits and 0.18 deg divergence slit was used. XRR data were simulated by using software from Panalytical. This commercial software is based on Parratt theory.[27] This method allowed us to determine thickness of the layer, electron density and roughness of the sample's surface and interface.[28,29] It should be mentioned that this method allows the determination of the global roughness of the sample.

X-ray photoelectron spectroscopy (XPS) measurements were made using a Scienta R4000 hemispherical analyzer (pass energy 200 eV) and Al K_α (1486.6 eV) excitation. The full width at half maximum (FWHM) of the $4f_{7/2}$ Au line measured at the same experimental condition was 1.1 eV. The energy scale was calibrated setting the carbon (C) 1s line at the position 285 eV. To avoid significant sample charging, the neutralization gun was used. Samples were measured as received. A significant amount of carbon was detected. To check if the carbon was present only at the surface the 5 min sputtering applying Ar^+ ion gun with 3 kV and 5 mA was performed.

Culture of Pre-Osteoblastic Mice Cell Line (MC3T3)

The MC3T3 cell line derived from European Collection of Authenticated Cell Cultures (ECACC). The cells were cultured under stable and aseptic conditions in a CO_2 incubator at 37°C and 95% humidity. The cells were cultured in complete growth medium (CGM) consisting of Minimum Essential Media Alpha (MEM-α, Gibco™ Thermo Fisher Scientific, Warsaw, Poland) supplemented with 10% FBS (Fetal Bovine Serum).

The medium was changed three times a week. Cultures were passaged using trypsin and EDTA solution (Trypsin-EDTA solution 0.25%, sterile-filtered Sigma Aldrich Sp. z o.o., Poznan, Poland) after reaching 90% confluence. The cells used for the experiment were subcultured for twenty passages (p20). A MiR-21 specific inhibitor (hsa-miR-21a-5p Anti-miR™ miRNA Inhibitor, Ambition, Thermo Fisher Scientific, Warsaw, Poland) was used according to the manufacturer's protocol as previously described.[30] The chosen concentration of a miR-21 specific inhibitor and ESCORT III transfection reagent was based on a screening test performed prior to the experiment (data not shown). The dilution of the miR-21 specific inhibitor was performed using Gibco™ MEM ALPHA MEDIUM no ascorbic acid (Thermo Fisher Scientific, Warsaw, Poland) to reach 30nM concentration. For the transfection, we used ESCORT III Transfection reagent (Sigma-Aldrich Sp. Z o. o. Poznan, Poland) in 1:100 concentration, according to the manufacturer's protocol. The cells were seeded on a 6-well plate in concentration 30,000 per well and divided into two experimental groups as follows: negative control of MC3T3 ($MC3T3_{NC}$) and $MC3T3_{inh21}$. The inhibition of miR-21 was confirmed using Two-tailed qPCR as well as miR-X assay, described below.

Cytocompatibility of ZrO_2^{ALD} Coatings

The experiment was carried out in 24-well plates coated with cover slips covered by ZrO_2^{ALD} coatings. Both $MC3T3_{NC}$ and $MC3T3_{inh21}$ were inoculated at a density equal to 30,000 cells per well. The cells were suspended in 0.5 mL of CGM. Cultures propagated in wells coated with blank cover slips (i.e. without coating) served as the control for the experiment. The cultures were propagated for 96 hrs.

The morphology and ultrastructure of cells in experimental and control cultures were analyzed based on the localization and distribution of the nuclei, cytoskeleton and mitochondrial network. The morphology of cells was investigated after 96 h using well-described protocols.[31,32] In order to visualize the mitochondria, cells were stained with MitoRed dye (Sigma Aldrich Sp. z o.o., Poznan, Poland) prepared in CGM at concentration (1:1000). The cultures were incubated with the dye in a CO_2 incubator for 30 mins. After staining, cells were fixed in 4% paraformaldehyde (PFA) for 30 mins at room temperature. Following fixation, cells were washed three times with HBSS (Hank's Balanced Salt Solution). Later, cell membranes were permeabilized with 0.2% Tween for 20 mins at room temperature. Next, cells were washed again with HBSS, as described above, and actin fibers were stained

with phalloidin-atto 488 prepared in HBSS (1:800). The staining was performed in a CO_2 incubator at 37°C for 30 mins, following which these cells were washed again with HBSS. Subsequently, biomaterials and cover slips were mounted on microscopic slides using a mounting medium (ProLong™ Diamond Antifade Mountant with DAPI, Thermo Fisher Scientific, Warsaw, Poland). 4′,6-Diamidine-2′-phenylindole dihydrochloride (DAPI) was used to visualize the nuclei. The prepared specimens were observed under a confocal microscope (Leica TCS SPE, Leica Microsystems, KAWA.SKA Sp. z o.o., Zalesie Gorne, Poland) and analyzed with Fiji is just ImageJ (ImageJ 1.52n, Wayne Rasband, National Institute of Health, USA). The proliferative activity of $MC3T3_{Inh21}$ and $MC3T3_{NC}$ was determined based on the distribution of cells in the cell cycle and DNA synthesis. The cell cycle was analyzed using a Muse® Cell Cycle Assay Kit (Merck, Warsaw, Poland). Cells were harvested after the experiment and fixed overnight using 70% ethanol. Further, cells were stained with the reagent provided with the kit. The cells were incubated with a reagent for 30 mins in the dark at room temperature. Next, the samples were analyzed using a Muse™ Cell Analyzer (Merck KGaA, Darmstadt, Germany).

Additionally, after 96hrs of the experiment, cells were harvested and seeded onto a 96-plate well in order to determine the influence of the coatings on cell proliferation. Analysis was performed using a colorimetric assay based on bromodeoxyuridine/5-bromo-2'-deoxyuridine (BrdU) incorporation. For this purpose, a BrdU Cell Proliferation ELISA Kit (Abcam, Cambridge, UK) was used according to the instructions provided with the kit and protocol described previously.[33] The absorbance was measured spectrophotometrically (Epoch, Biotek, Bad Friedrichshall, Germany) at a wavelength of 450 nm and 550 nm as a reference wavelength.

A Muse™ Cell Analyzer was used to determine cell viability and mitochondrial membrane potential. After culture, cells were harvested using trypsin solution and stained with Muse® Annexin V and Dead Cell Assay Kit following the protocol provided by the manufacturer (Merck, Warsaw, Poland) to evaluate necrosis and apoptosis in the experimental cultures. Staining with a MitoPotential Kit (Merck, Warsaw, Poland) performed according to the manufacturer's protocol, provided information on the MC3T3 mitochondrial membrane potential. Each measurement was performed a minimum of three times.

Total RNA was isolated using the phenol-chloroform method.[34] For this purpose, after the experiment cells were homogenized, 1 mL of Extrazol® (Blirt DNA Gdansk, Gdansk, Poland) was used. The protocol of RNA isolation was performed according to the instructions of the manufacturer. The RNA intact was determined based on spectrophotometric measurement (Epoch, Biotek, Bad Friedrichshall, Germany) at a wavelength of 260/280. The obtained RNA was used for the cDNA synthesis in reverse transcription (RT). Before each reaction, total RNA was purified by DNAse I digestion. Reaction was performed using PrecisionDNAse kit (PrimerDesign, BLIRT S.A. Dzial DNA-Gdansk, Gdansk, Poland) using the well-established protocol. For two-tailed qPCR, 50ng/mL of RNA was used for cDNA synthesis, while for mRNA detection 500 ng of RNA was used. The details of the protocols were described earlier.[35,36] The reverse transcription was performed using a Tetro cDNA Synthesis Kit (Bioline Reagents Ltd., London, United Kingdom) according to the protocol provided by the manufacturer. Additionally, cDNA was synthesized from 375 ng of total RNA using Mir-X™ miRNA First-Strand Synthesis Kit (Takara Bio Europe, Saint-Germain-en-Laye, France). All reactions included no-RT control. Both DNA digestion and reverse transcription were performed in a T-100 Thermal Cycler (Bio-Rad Poland Sp. z. o.o., Warsaw, Poland). The matrices obtained in reverse transcription were used for quantitative PCR (final volume 10 µL) with a SensiFast SYBR & Fluorescein Kit (Bioline Reagents Ltd., London, United Kingdom). The reaction conditions were described previously.[35,37,38] The list of primers is presented in Supplementary Material. The average fold change in the gene expression was calculated using the RQ_{MAX} algorithm, ie scaled to the sample having the lowest expression and converted into log2 scale as described previously.[35] The analysis was performed in relation to the housekeeping gene-GAPDH for target genes, and U6snRNA for miRNA.

Statistical Analysis

The mean was calculated from a minimum of three measurements. The data obtained were analyzed using GraphPadPrism 5 software (La Jolla, CA, USA). Differences between groups were determined using parametric assays, unpaired Student's *t*–test or one-way analysis of variance (ANOVA). Differences with a probability of $p < 0.05$ were considered to be significant.

Results

Physicochemical Properties of the ZrO_2^{ALD} Coatings

The ZrO_2^{ALD} layers deposited on silicon substrates were used for the SEM investigation shown in Figure 1A. Analysis of top-view SEM images (confirmed by lack of signal by the XRD investigations, not shown here) indicates the amorphous nature of the coating and the high quality of the resulting layer, without noticeable cracks or unevenness (Figure 1A, top panel). The homogeneous thickness on the SEM (CS) image was observed as shown in Figure 1A, bottom panel.

In the XPS wide scan, only Zr, O and C signals were detected. The analysis of the Zr 3d and O 1s narrow scan lines proved that in the as-grown sample only one chemical bond of Zr was detected (183 eV) and two kinds of O bonds. The binding energy of the main oxygen line was 530.8 eV. The binding energies of both elements are very close to those reported in the reference tables and spectra (182.5 and 530.4 eV, respectively) indicating a small charging shift.[39,40] The second compound of oxygen has its bonding energy shifted by 1.8 eV from the main line, which is common for absorbed water and adventitious carbon contaminations. The FWHM of spin orbit doublet is 1.44 eV, only slightly wider than that reported in the reference tables measured with monochromatic excitation. The ratio of the Zr to O (1:1.75) resulting from XPS measurements indicated that the surface is depleted of oxygen. A significant amount of C (23%) was detected at the surface. To check if this is only surface contamination due to exposure to air, 5 mins of Ar sputtering was performed. The amount of C was reduced to ~3% but due to preferential sputtering of oxygen, the ratio of oxygen to zirconium decreased to 1.4. This was evidence of the structural disorder introduced by sputtering, as was reported previously.[41]

The results of the simulation of curve fitting to the XRR measurement data are shown in Figure 1B. The simulation model included the presence of interlayers between the Si substrate and the coating and took into account possible surface contamination. The estimated ZrO_2^{ALD} film thickness (83.7 nm) corresponds well with estimations from SEM cross-sections and reflectometry measurement, using a NanoCalc spectrometer (84 nm). A thin layer (2.7 nm) between the Si substrate and the ZrO_2^{ALD} layer was observed, which is due to the forming of an ultra-thin layer of native oxide when the substrate comes into contact with the air or with water during the washing processes.[42,43] On the ZrO_2 surface, we observed a 3 nm thick layer due to the presence of surface contaminants, e.g. carbon formed after contact with air, as confirmed by the XPS measurements. The roughness of the ZrO_2^{ALD} was calculated as 3.3 nm.

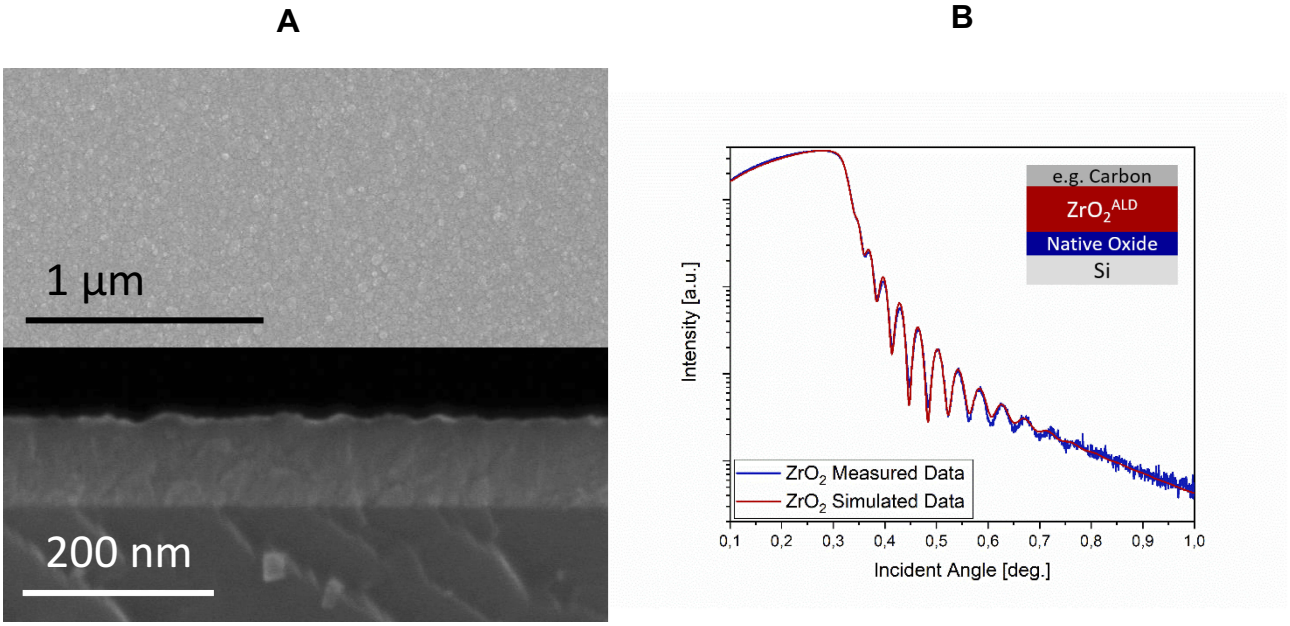

Figure 1 The SEM images of ZrO_2^{ALD} coatings (**A**). The top-view image (top panel) shows the homogeneity of the coating, the cross-section image (bottom panel) indicates the even thickness distribution of the layer. Measured and simulated data XRR (X-ray Reflectivity) are shown (**B**). The insert shows the model used for simulation to estimate thickness and electron density of the obtained coating.

Biological Properties of the Coatings

The Influence of ZrO_2^{ALD} Coatings on Cells Morphology and Ultrastructure Organization

The morphology of cells and their ultrastructure were analyzed after 96h of experiment. Observation revealed that both in experimental and control culture cells maintained proper morphology. In all cultures, MC3T3 were characterized by heterogenous appearance, typical for the early stage of their differentiation. Both multipolar fibroblast-like cells and round or oval cells were observed. The nuclei were located centrally within the cell. No formation of apoptotic bodies was noted. Inhibition of miR-21 in cultures on plain cover slip, as well as on biomaterial with ZrO_2^{ALD} coating resulted in formation of more complex intracellular connections with visible projections, i.e. lamellipodia and filopodia. However, the architecture of growth was more complex in cultures on ZrO_2^{ALD} coatings, both in $MC3T3_{NC}$ and in $MC3T3_{inh21}$. Additionally, the cells cultured on ZrO_2^{ALD} coatings had well-developed mitochondrial networks visualized after mitoRed staining (Figure 2).

The Influence of ZrO_2^{ALD} Coatings on Cells Proliferation

The proliferative activity of MC3T3 was analyzed based on cell distribution in the cell cycle as well as based on the incorporation of BrdU during the S-phase of the cell cycle (Figure 3). Analysis revealed that inhibition of miR-21 may affect the proliferative activity of cells, decreasing cell numbers in the S phase (Figure 3A and B). This was evidenced especially in cultures propagated on ZrO_2^{ALD} coatings. The distribution of cells in the cell cycle showed that inhibition of miR-21 in cultures on plain cover slips also significantly reduces the cells in the G2/M phase. $MC3T3_{inh21}$ propagated on ZrO_2 coatings were characterized by a significant decrease of cells in the S-phase. This status was correlated with an increase of the population shifted toward the G0/G1 phase and with a decrease of cells in the G2/M phase (Figure 4A and B). In turn, the results of BrdU assay (Figure 3C) indicated that ZrO_2^{ALD} had a slight pro-proliferative effect on pre-osteoblasts.

The Influence of ZrO_2^{ALD} Coatings on Mitochondrial Membrane Potential

Analysis of mitochondrial membrane potential performed using a MUSE Cell Analyzer showed that MC3T3 propagated on ZrO_2^{ALD} coatings were characterized by higher mitochondrial potential, when compared to cultures on cover slips (Figure 4A and B). Additionally, it was shown that inhibition of miR-21 in cultures maintained on plain cover slips may influence the decrease of mitochondrial activity. In turn, the $MC3T3_{inh21}$ propagated on ZrO_2^{ALD} cultures were distinguished by increased mitochondrial membrane potential (Figure 4A and B). The results were also confirmed by the analysis of metabolic activity performed using an Alamar Blue assay (Figure 4C). The analysis of cell metabolism during the adaptive phase of their growth showed that inhibition of miR-21 may affect the activity of cells, both in cultures on plain cover slip, and on the biomaterial. The decreased metabolic activity of $MC3T3_{inh21}$ was maintained in cultures on plain cover slip, which was noticed after 72 and 96 hrs of culture. In turn, MC3T3 propagated on biomaterial showed increased activity at later stages of culture.

The Influence of ZrO_2^{ALD} Coatings on Apoptosis Profile

The apoptosis profile was established based on cell distribution after Annexin V/7-AAD staining. Analysis revealed that cultures propagated on ZrO_2^{ALD} coatings were characterized by increased apoptosis. In cultures maintained on plain cover slip, the inhibition of miR-21 was associated with increased viability of cells. The opposite tendency was noted in $MC3T3_{inh21}$ cultures propagated on ZrO_2^{ALD} coatings (Figure 5A–C). Additionally, analysis of apoptosis was performed based on the expression profile of genes associated with cell death. The expression of mRNA for *Bcl-2*, *Bax*, *p53* and *p21* was tested. The obtained results indicated increased expression of all transcripts, which confirms the cytotoxic effect of ZrO_2^{ALD} coatings toward MC3T3 (Figure 5D–G).

ZrO_2^{ALD} Coatings Upregulate Osteogenic Genes Expression in MC3T3 Cells with and Without mir-21 Inhibition (mRNA/miRNA Level)

The influence of ZrO_2^{ALD} coatings on osteogenesis was evaluated based on the expression profiles of genes and miRNA crucial in osteogenesis, including *Coll-1, Opn*, *Ocl* and *Runx-2* (Figure 6A–D). The ZrO_2^{ALD} induced higher mRNA levels of osteogenic markers also in cells with decreased activity of miR-21 (Figure 6). The expression of all the mentioned transcripts was noticeably higher in cultures propagated on ZrO_2^{ALD}, based on the obtained results. Subsequently, the transcript levels of miR-7, miR-21 and miR-223 were tested. Analysis showed that miR-21 inhibition was correlated with downregulation of miR-7, regardless of the culture conditions (Figure 6E and F). The

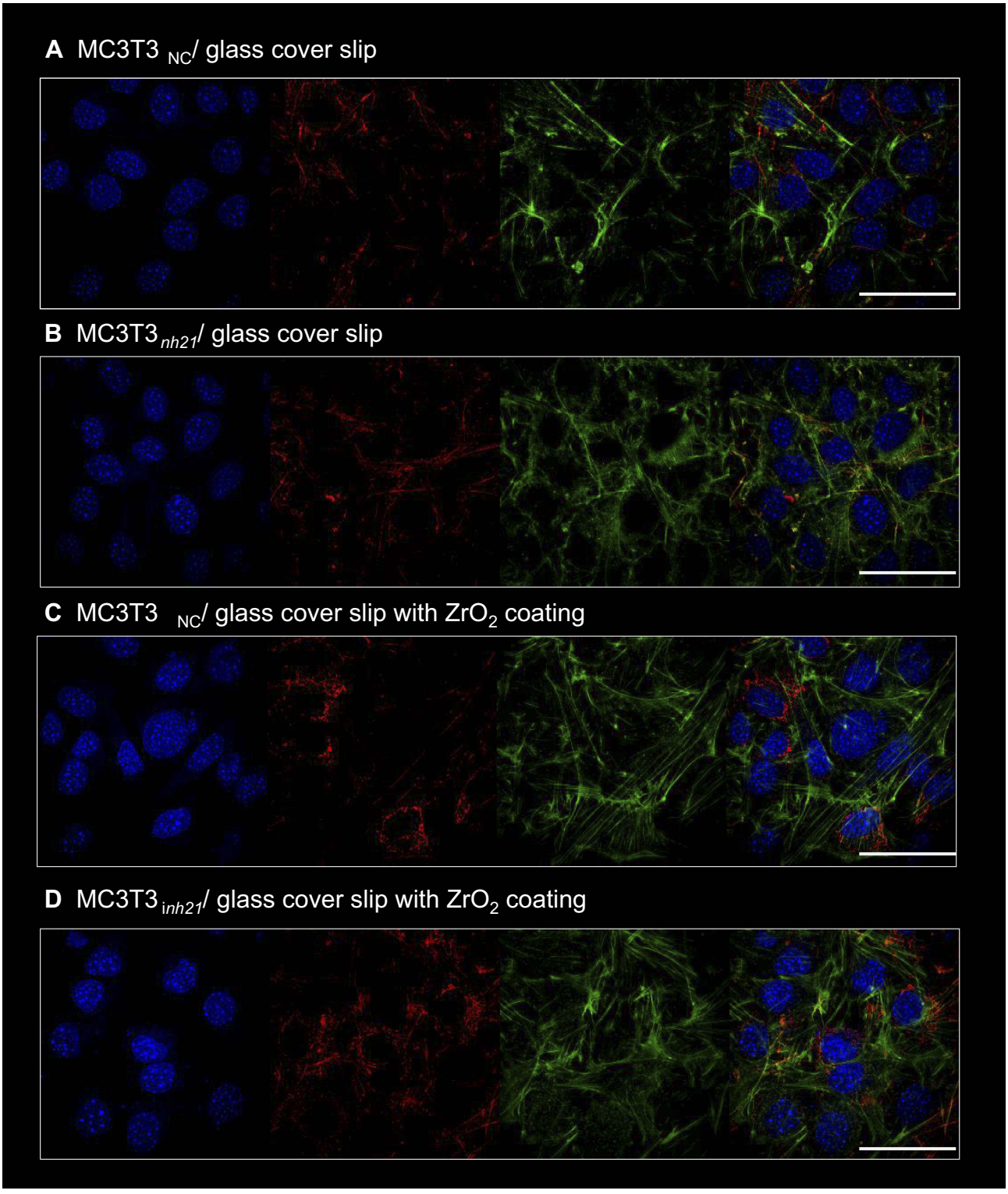

Figure 2 The morphology of pre-osteoblasts cultured in control cultures (glass cover slip, **A** and **B**) and cultured on ZrO_2 coatings (**C, D**). The MC3T3 model of pre-osteoblast was used – both $MC3T3_{NC}$ and $MC3T3_{inh21}$. The cells were stained with DAPI, in order to visualize the nuclei (blue). The mitochondria network is visualized after MitoRed staining (red), while cytoskeleton with phalloidin atto488 (green). The cells were observed using confocal microscopy under 60-fold magnification. Scale bar is 50 μm, included on the merged photograph.

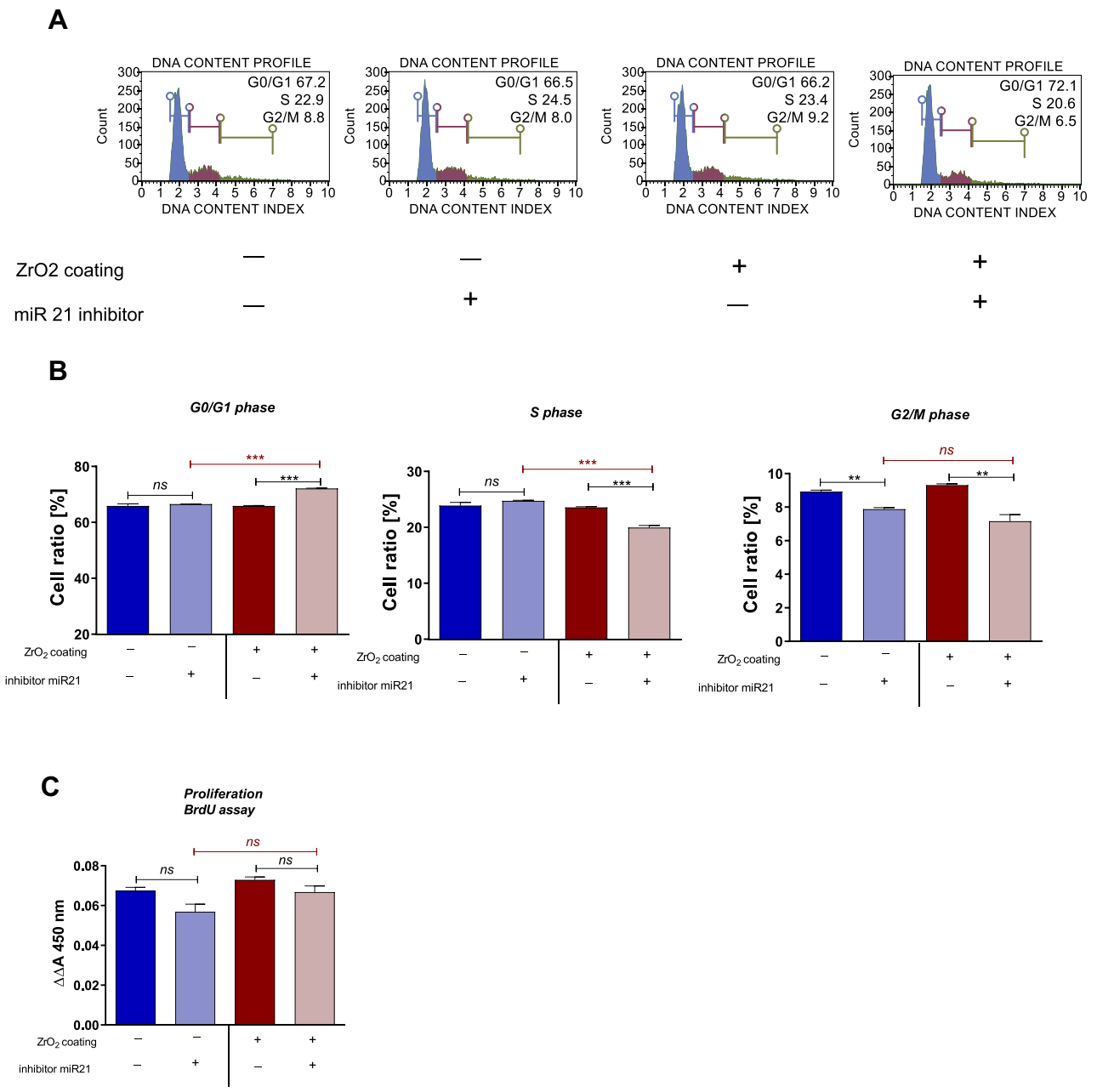

Figure 3 Results of analysis of proliferative status of MC3T3 cells in cultures on substrate with and without ZrO_2^{ALD} coating. (**A**) Representative images showing the distribution of cells within the cell cycle. (**B**) Statistical analysis of the results obtained for cytometric measurements. (**C**) Statistical analysis of results obtained in BrdU assay. An asterisk marks a statistically significant difference (***p < 0.001; **p < 0.01). Differences without significant impact were indicated using the symbol ns (not significant).

levels of pro-osteogenic miR-223 were increased in cultures propagated on ZrO_2^{ALD} coating (Figure 6G). The presented results confirm the pro-osteogenic properties of ZrO_2^{ALD}.

Discussion

Currently, medicine is faced with the urgent need to establish new methods of treatment that would improve the regenerative potential of an organism. This is closely connected with the ongoing senescence of modern societies followed by a growing prevalence of lifestyle diseases, including osteoporosis. Additionally, trauma in geriatric patients increases with age; thus, there is a great need to develop new therapeutic strategies promoting healing and having a bridging function, enhancing functional recovery. Tissue engineering combined

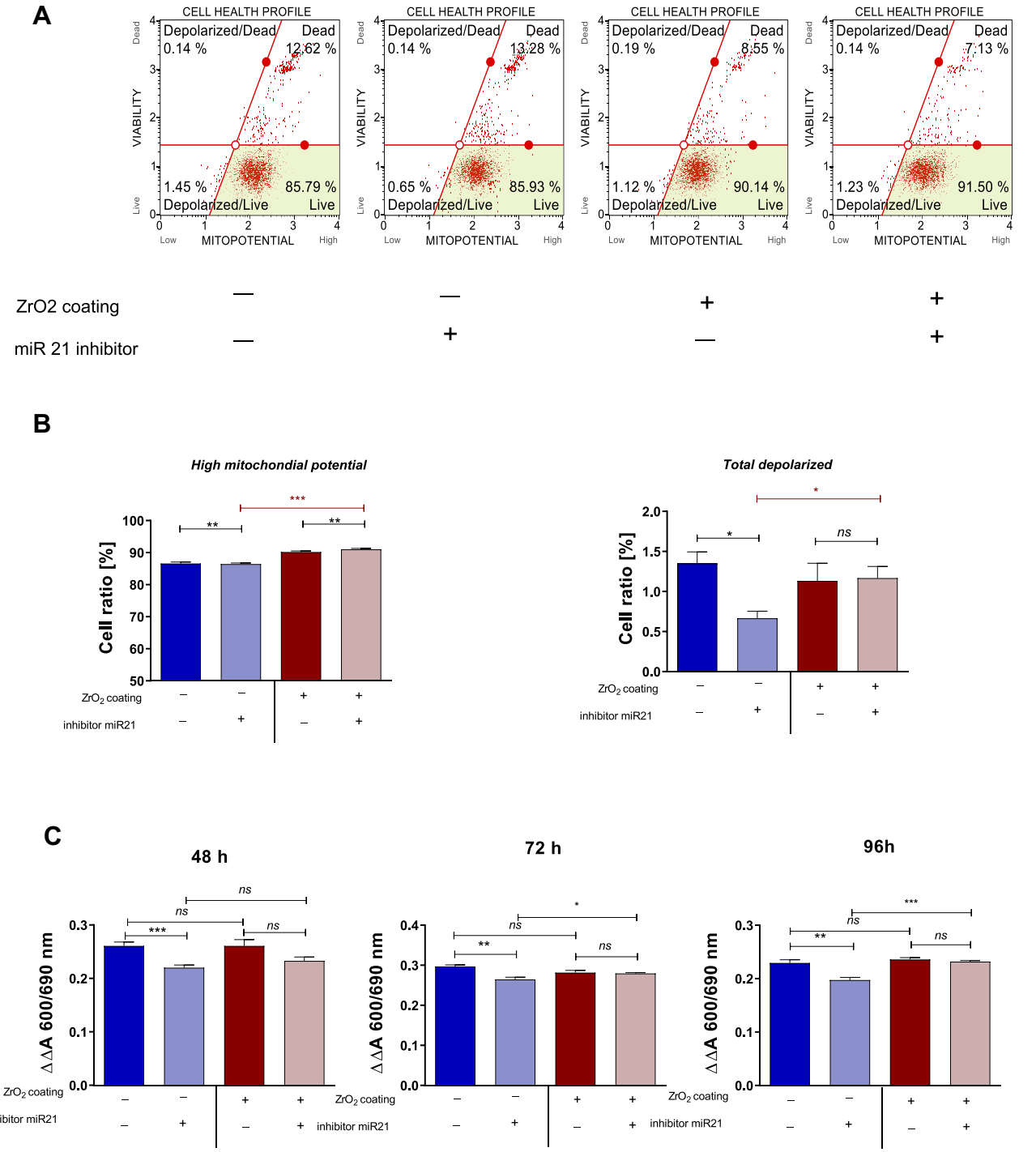

Figure 4 Results of analysis of metabolic activity of MC3T3 in cultures on substrate with and without ZrO_2 coating. (**A**) Representative images showing the distribution of cells based on mitochondrial membrane potential (**B**) Statistical analysis of the results obtained for cytometric measurements. (**C**) Statistical analysis of results obtained for Alamar blue assay. An asterisk marks a statistically significant difference (***p < 0.001; **p < 0.01 and *p<0.05). Differences without significant impact were indicated using ns.

with biomaterials engineering helps in finding new solutions in terms of regenerative medicine, foremost in orthopedics. In the past few years, next to titanium, zirconium oxide has become the focal point of numerous works of published research due to its beneficial mechanical characteristics and the positive effect it exerts on osteogenesis. The purpose of this study was to determine if ZrO_2 coatings could be used in the development of new, highly biocompatible implants with application in bone fracture treatment, especially in patients with

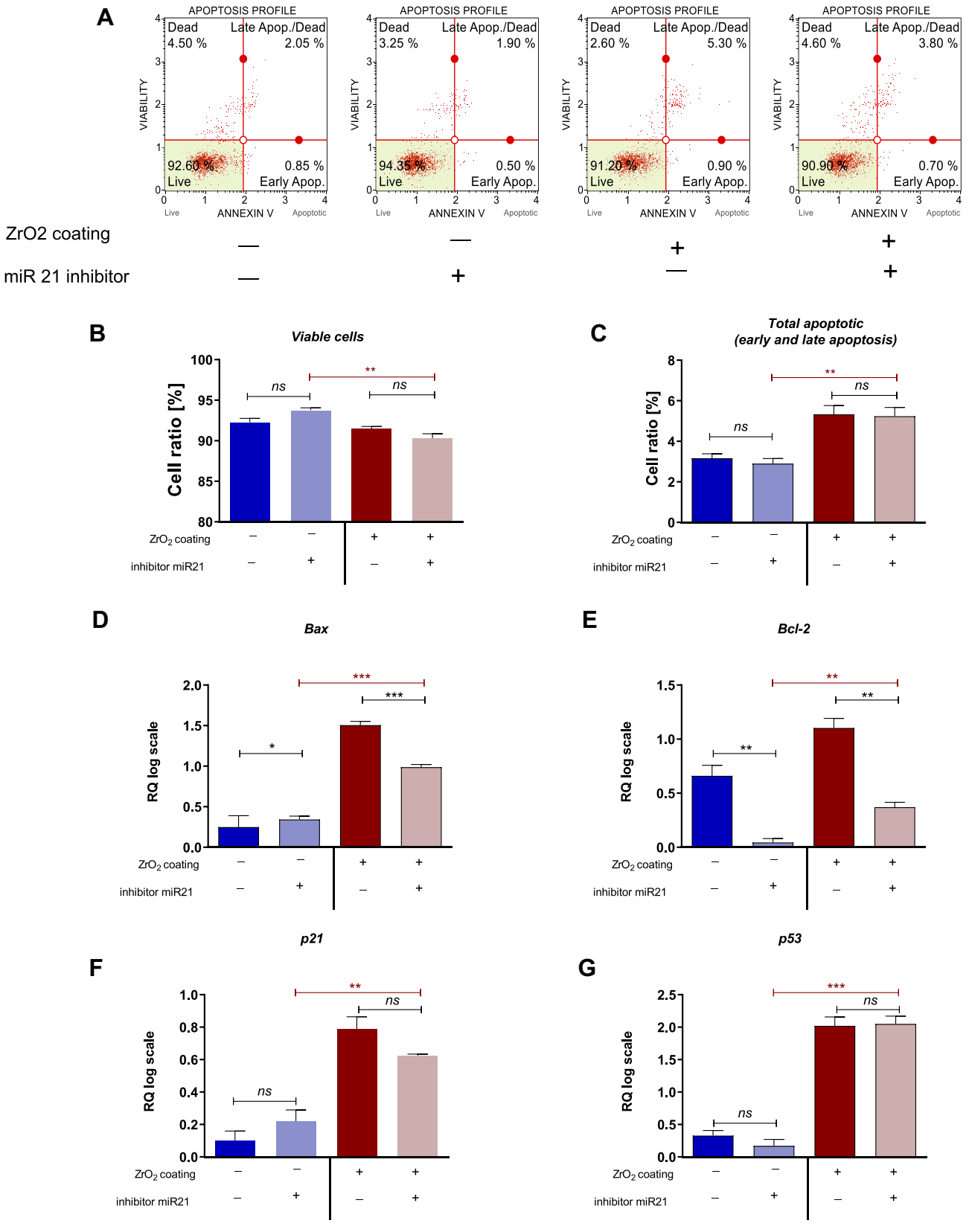

Figure 5 Results of apoptosis analysis in control cultures (glass substrate) and experimental cultures (substrate with ZrO_2^{ALD}). (**A**) Representative images showing the distribution of cells based on their viability. (**B, C**) Statistical analysis of the results obtained for cytometric measurements. (**D**–**G**) Analysis of transcript levels for genes associated with apoptosis. An asterisk marks a statistically significant difference (***p < 0.001; **p < 0.01 and *p<0.05). Differences without significant impact were indicated using ns.

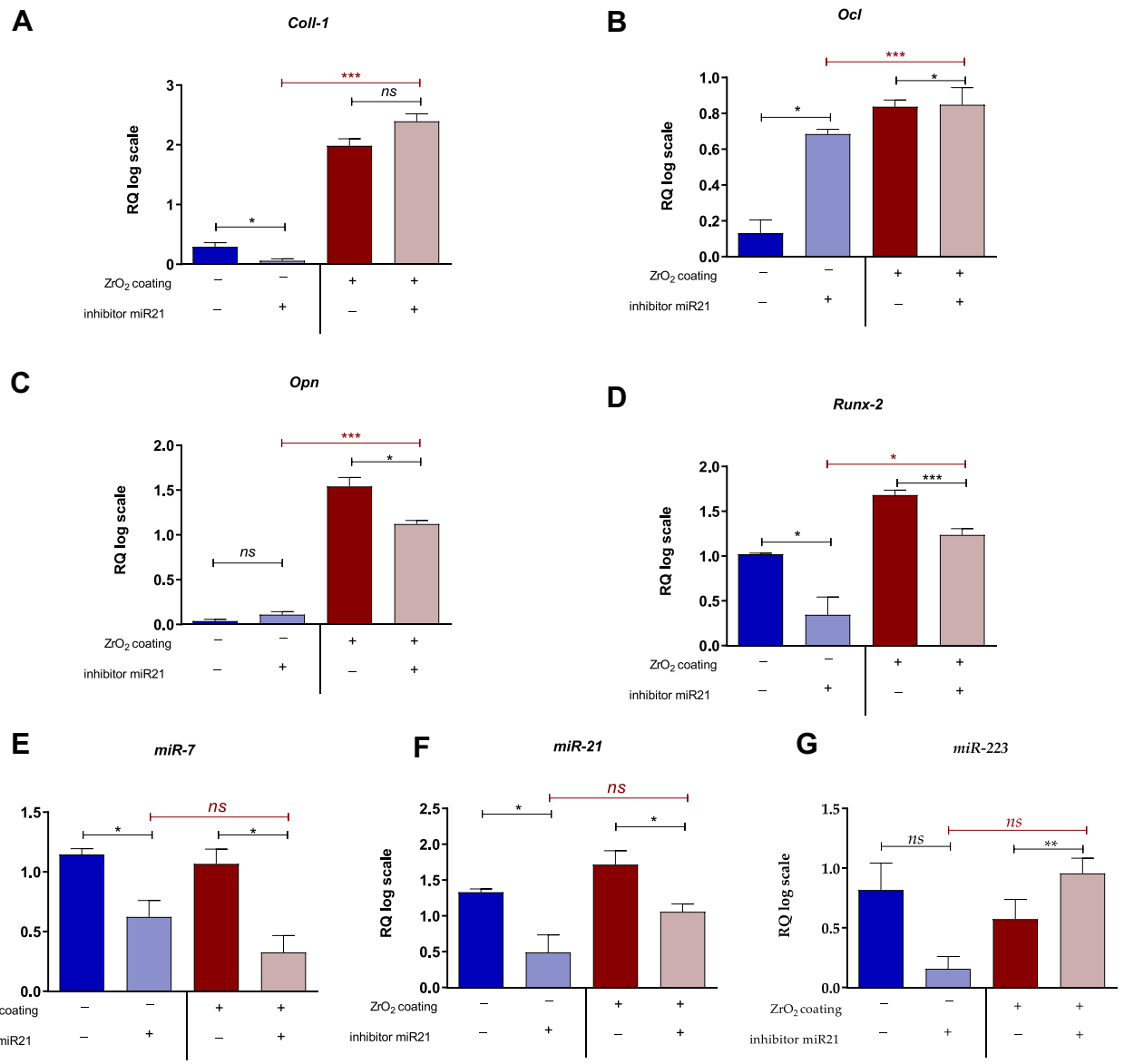

Figure 6 Transcript levels of osteogenic markers. The analysis included measurement of mRNA level for *Coll-1* (**A**), *Ocl* (**B**), *Opn* (**C**) and *Runx-2* (**D**). The miRNA levels were also established. MiR-7 (**E**) and miR-21 (**F**) revealed a similar expression pattern. The miR-223 (**G**) was significantly increased in $MC3T3_{inh21}$ propagated on ZrO_2 coating. An asterisk marks a statistically significant difference (***p < 0.001; **p < 0.01 and *p<0.05). Differences without significant impact were indicated using ns.

lowered regenerative potential, e.g. senile osteoporosis. For this purpose, we created ZrO_2 coated coverslips using the ALD method which has gained attention as a precise technique allowing to create a uniform, thin film on various materials in layer-by-layer fashion.

The unquestionable advantage of ALD technology is the possibility of the growth of uniform and conformal layers,[9] which in the present work was confirmed by the SEM study of the ZrO_2^{ALD} coating under consideration.[11] The measurement was made for the films deposited on Si substrate but, based on our experience, the ALD method allows also the deposition of high-quality film growth on other substrates, including glass. The ZrO_2^{ALD} layer density (5.5 g/cm^3), as simulated by the XRR data measurement, corresponds well to the bulk density of ZrO_2 (5.68 g/cm^3) and confirms the relatively high quality of the ALD layer.

Carbon was found in the deposited films, as observed by XPS investigations. Pollution at the level of ~3% might be a result of using organic precursors rich in carbon (TDMA-Zr in the present work). In fact, the presence of carbon in the films is known for various coatings obtained by ALD technology, e.g. Al_2O_3.[44] The observed oxygen deficiency in the layer (non-stoichiometric oxide) indicates

the formation of defects during the deposition process and/or unintentional dopants. In the present case, this may be carbon contamination as mentioned above. The non-stoichiometric nature of ZrO_2 was tested for its effect on the electrical properties of the films.[45] Regarding the biological properties in conjunction with the stoichiometry of the ZrO_2 coatings, no studies in this field have been reported to date.

To assess the possible pro-osteogenic properties of acquired ZrO_2^{ALD} coatings, an experimental MC3T3 cell culture was used. The cells were transfected with miR-21 inhibitor to obtain a cell line with disturbed osteogenic potential. The selection of the miR-21 molecule as a target was made based on its crucial role as a regulator of various osteogenic markers, including Runx-2, which is a key molecule mediating the differentiation of osteoblasts. Additionally, several studies showed that miR-21 levels are decreased in bone tissue and serum of patients with osteoporosis.[25] Lowered levels of miR-21 correspond with lowered bone mineral density (BMD) and thus miR-21 began to be acknowledged as a potential biomarker of bone diseases, such as osteoporosis and osteopenia.[46] Since miR-21 was proven to affect the differentiation and proliferation of both osteoblasts and osteoclasts, the mechanism underlying its pro-osteogenic activity is very complex and not fully explained. However, it was shown that by positively mediating MMP-2, MMP-9, MMP-M1 and downregulating pro-apoptotic TNF-α expression miR-21 may promote osteoblast differentiation and proliferation.[47] The performed analysis of the MC3T3 cycle confirmed that miR-21 may regulate the proliferative activity of pre-osteoblasts. Cells transfected with miR-21 inhibitor were characterized by a shift towards the G1/0 phase with decrease of population in both the S and the G2/M phase. Furthermore, it was also proven that down-regulation of miR-21 is associated with osteoclast differentiation and as such may contribute to osteoporosis progression.[48] Zirconia-based coatings reportedly improve the osteointergration of metallic implants, which is associated with increased adhesion of progenitor cells to the biomaterial surface, as was previously described in both experimental models: in vivo and in vitro.[5,49] However, da Cota Fernandes et al[20] presented a contradictory conclusion, stating that ZrO_2 may weaken pre-osteoblast adhesion by enhancing extracellular matrix remodelling as a precedence to intensified proliferation. Our data showed that zirconium improves both proliferation and adhesion of pre-osteoblast. The ZrO_2^{ALD} coatings affect the architecture of pre-osteoblast growth, promoting the formation of intracellular connections, crucial for proper differentiation and formation of the extracellular matrix network.[50] Rizzi et al[49] also observed that the MC3T3 pre-osteoblasts growing on screws coated with zirconium were characterized by higher proliferative potential.[49] Similarly, the proliferation of human osteoblast cells (HOB) was increased in response to zirconia.[20,51] All collected evidence is in line with our results and proves that biological activity of zirconia is related to its pro-proliferative potential. The proliferation of progenitor cells during the process of differentiation is modulated and should be correlated with the metabolic status of cells. In this study, we have shown that miR-21 inhibition has a negative impact on pre-osteoblast metabolic activity, while ZrO_2 may alleviate decreased metabolism. The attenuated metabolic activity of osteoblasts disturbs the homeostasis of bone and may result in osteoporosis. Thus, obtained results are promising in light of new treatment strategies for the treatment of osteoporotic fractures.[52] The increased metabolic activity of pre-osteoblast cultured on ZrO_2^{ALD} coatings was associated with developed mitochondrial networks and improved mitochondrial membrane potential. However, as was also previously observed by Ye et al[53] zirconium nanoparticles may increase Reactive Oxygen Species (ROS) generation, which may lead to the induction of apoptosis in pre-osteoblastic cells, but this mechanism greatly depends on the concentration of nanoparticles. This study may explain the increased number of cells with total depolarized mitochondrial membranes and increased apoptosis in cultures on ZrO_2^{ALD} coatings. The observed cytotoxic effect of ZrO_2^{ALD} coatings can be described as mild, as it did not affect cell morphology and proliferative status. ROS generation induced by ZrO_2 may trigger miR-21 overexpression, which was previously shown using the model of human umbilical vein endothelial cells (HUVEC) during oscillating and high glucose exposures. This may explain the increased expression of mRNA for essential osteogenic markers, such as Coll-1, OCL, OPN and Runx-2. The obtained data indicate that ZrO_2^{ALD} is able to enhance pro-osteogenic gene expression, possibly via upregulating mir-21 expression that targets Runx-2, promoting osteogenic differentiation. We have also indicated that pre-osteoblasts with inhibited activity of miR-21 were also characterized by decreased levels of miR-7. The role of miR-7 in the course of osteogenesis is not well studied; however, it may be relevant in terms of metabolic activity of differentiating

pre-osteoblasts, as well as may modulate osteoblasts viability.[54] The expression profile of miR-223 is in good agreement with mRNA levels of osteogenic markers. Increased levels of miR-223 were noted in MC3T3 cultures propagated on ZrO_2^{ALD} coatings. MiR-223 was recently identified as a key modulator of osteoblastic differentiation in MC3T3-E1 cells, which targets histone deacetylase 2 (HDAC2).[55]

To summarize, the obtained ZrO_2^{ALD} coatings are cytocompatible toward the MC3T3 osteoblastic cell line. The coatings promote the metabolic potential and may mitigate the effect of miR-21 inhibition, increasing expression of osteogenic markers, both at mRNA and miRNA level.

Conclusion

Physical and chemical analysis indicated the presence of an amorphous zirconium oxide layer, grown by ALD technology, with a thickness of 84 nm. The obtained coating is characterized by a high homogeneity and a low roughness. The ALD technology allowed us to obtain uniform thickness distribution on the surface of the substrate. The only chemical elements detected in the investigated thin film are zircon, oxide and carbon. The detected carbon was mostly due to surface contamination. The XPS measurement after Ar bombardment shows that the concentration of carbon dropped dramatically, and the value of inner carbon pollution may be about 3 Atom %. This may be related to the precursors used in the ALD process. A slight nonstoichiometry of the samples was observed, indicating the presence of oxygen defects in the film.

The obtained coatings are highly cytocompatible, which was shown using the model of MC3T3 pre-osteoblasts. The coatings have biomimetic properties, promoting cell adhesion and spreading. The obtained coatings improved the metabolism of cells, increasing the mitochondrial membrane potential and the development of mitochondrial networks. Moreover, ZrO_2^{ALD} coatings promoted increased expression of typical osteogenic markers, which was confirmed using $MC3T3_{inh21}$ Bearing these results in mind, ZrO_2^{ALD} coatings with pro-osteogenic potential may find application in bone tissue engineering.

Abbreviations

ALD, atomic layer deposition; ALP, alkaline phosphatase; ASC, adipose tissue-derived stromal cells; BAX, Bcl-2-associated X protein; BCL-2, B-cell lymphoma 2; BMP-2, bone morphogenetic protein 2; BMSC, bone-marrow multipotent stromal cells; BrdU, bromodeoxyuridine/5-bromo-2'-deoxyuridine; CGM, complete growth medium; Coll-1, collagen type 1; ECM, extracellular matrix; GAPDH, glyceraldehyde 3-phosphate dehydrogenase; HBSS, Hank's Balanced Salt Solution; HIF-1α, hypoxia-inducible factor-1α; HOB, human osteoblast cells; MC3T3, pre-osteoblastic mice cell line; $MC3T3_{inh21}$, MC3T3 cells with miR21 inhibitor; $MC3T3_{NC}$, negative control; miRNA/miR, micro ribonucleic acid; MMP, matrix metallopeptidases; mRNA, messenger ribonucleic acid; MSC, multipotent cells of mesenchymal origin; ns, not significant; OCL, osteocalcin; OPN, osteopontin; PCR, polymerase chain reaction; PFA, paraformaldehyde; ROS, Reactive Oxygen Species; RT, reverse transcriptase; Runx-2, runt-related transcription factor 2; SEM, Scanning Electron Microscope; TDMA-Zr, Tetrakis (dimethylamido) zirconium; TNF-α, tumor necrosis factor α; VEGF, vascular endothelial growth factor; XPS, X-ray photoelectron spectroscopy; XRR, X-ray reflectometry; ZrO_2, zirconium oxide; ZrO_2^{ALD}, zirconium oxide thin film obtained by ALD technology.

Acknowledgments

Financial support from the National Science Centre over the course of the realization of the project Harmonia 10 titled "New, two-stage scaffolds based on calcium nanoapatite (nHAP) incorporated with iron nanotoxides (Fe_2O_3 /Fe_3O_4) with the function of controlled release of miRNA in a static magnetic field for the regeneration of bone fractures in osteoporotic patients" (Grant No. UMO 2017/26/M/NZ5/01184) is gratefully acknowledged.

Disclosure

Dr Agnieszka Śmieszek reports grants from National Science Centre (Poland), during the conduct of the study. The authors report no other conflicts of interest in this work.

References

1. Ghiasi MS, Chen J, Vaziri A, Rodriguez EK, Nazarian A. Bone fracture healing in mechanobiological modeling: a review of principles and methods. *Bone Rep*. 2017;6:87–100. doi:10.1016/j.bonr.2017.03.002
2. Einhorn TA, Gerstenfeld LC. Fracture healing: mechanisms and interventions. *Nat Rev Rheumatol*. 2015;11(1):45–54. doi:10.1038/nrrheum.2014.164
3. Gómez-Barrena E, Rosset P, Lozano D, Stanovici J, Ermthaller C, Gerbhard F. Bone fracture healing: cell therapy in delayed unions and nonunions. *Bone*. 2015;70:93–101. doi:10.1016/j.bone.2014.07.033
4. Piconi C, Maccauro G. Zirconia as a biomaterial. *Biomaterials*. 1997;1:1–25.
5. Sollazzo V, Pezzetti F, Scarano A, et al. Zirconium oxide coating improves implant osseointegration in vivo. *Dent Mater*. 2008;24(3):357–361. doi:10.1016/j.dental.2007.06.003

6. Hausmann DM, Kim E, Becker J, Gordon RG. Atomic layer deposition of hafnium and zirconium oxides using metal amide precursors. *Chem Mater*. 2002;14(10):4350–4358. doi:10.1021/cm020357x
7. Godlewski M, Gierałtowska S, Wachnicki Ł, et al. High-k oxides by atomic layer deposition—applications in biology and medicine. *J Vac Sci Technol a Vac Surf Film*. 2017;35(2):021508. doi:10.1116/1.4974314
8. Suntola T. *Atomic Layer Epitaxy*. Espo: Microchemistry Ltd; 1989.
9. Ritala M, Leskelä M. Atomic layer epitaxy - a valuable tool for nanotechnology? *Nanotechnology*. 1999;10(1):19–24. doi:10.1088/0957-4484/10/1/005
10. Miikkulainen V, Leskelä M, Ritala M, Puurunen RL. Crystallinity of inorganic films grown by atomic layer deposition: overview and general trends. *J Appl Phys*. 2013;113(2):021301. doi:10.1063/1.4757907
11. Gieraltowska S, Wachnicki L, Witkowski BS, Mroczynski R, Dluzewski P, Godlewski M. Characterization of dielectric layers grown at low temperature by atomic layer deposition. *Thin Solid Films*. 2015;577:97–102. doi:10.1016/j.tsf.2015.01.059
12. Knez M, Nielsch K, Niinistö L. Synthesis and surface engineering of complex nanostructures by atomic layer deposition. *Adv Mater*. 2007;19(21):3425–3438. doi:10.1002/adma.200700079
13. Cremers V, Puurunen RL, Dendooven J. Conformality in atomic layer deposition: current status overview of analysis and modelling. *Appl Phys Rev*. 2019;6(2):021302. doi:10.1063/1.5060967
14. Nilsen O, Fjellvåg H, Kjekshus A. Growth of calcium carbonate by the atomic layer chemical vapour deposition technique. *Thin Solid Films*. 2004;450(2):240–247. doi:10.1016/j.tsf.2003.10.152
15. Putkonen M, Sajavaara T, Rahkila P, et al. Atomic layer deposition and characterization of biocompatible hydroxyapatite thin films. *Thin Solid Films*. 2009;517(20):5819–5824. doi:10.1016/j.tsf.2009.03.013
16. Holopainen J, Kauppinen K, Mizohata K, et al. Preparation and bioactive properties of nanocrystalline hydroxyapatite thin films obtained by conversion of atomic layer deposited calcium carbonate. *Biointerphases*. 2014;9(3):031008. doi:10.1116/1.4889975
17. Niinistö L, Päiväsaari J, Niinistö J, Putkonen M, Nieminen M. Advanced electronic and optoelectronic materials by atomic layer deposition: an overview with special emphasis on recent progress in processing of high-k dielectrics and other oxide materials. *Phys Status Solidi Appl Res*. 2004;201(7):1443–1452. doi:10.1002/pssa.200406798
18. Seppälä S, Vehkamäki M, Mizohata K, et al. Comparative study on the use of novel heteroleptic cyclopentadienyl-based zirconium precursors with H2O and O3 for atomic layer deposition of ZrO2. *J Vac Sci Technol A*. 2019;37(2):020912. doi:10.1116/1.5079539
19. Leskelä M, Ritala M. Atomic layer deposition (ALD): from precursors to thin film structures. *Thin Solid Films*. 2002;409(1):138–146. doi:10.1016/S0040-6090(02)00117-7
20. da Cota Fernandes CJ, Ferreira MR, Bezerra FJB, Zambuzzi WF. Zirconia stimulates ECM-remodeling as a prerequisite to pre-osteoblast adhesion/proliferation by possible interference with cellular anchorage. *J Mater Sci Mater Med*. 2018;29(41). doi:10.1007/s10856-018-6041-9
21. Śmieszek A, Donesz-Sikorska A, Grzesiak J, Krzak J, Marycz K. Biological effects of sol–gel derived ZrO_2 and SiO_2 /ZrO_2 coatings on stainless steel surface—in vitro model using mesenchymal stem cells. *J Biomater Appl*. 2014;29(5):699–714. doi:10.1177/0885328214545095
22. Śmieszek A, Szydlarska J, Mucha A, Chrapiec M, Marycz K. Enhanced cytocompatibility and osteoinductive properties of sol–gel-derived silica/zirconium dioxide coatings by metformin functionalization. *J Biomater Appl*. 2017;32(5):570–586. doi:10.1177/0885328217738006
23. Sivaraman K, Chopra A, Narayan AI, Balakrishnan D. Is zirconia a viable alternative to titanium for oral implant? A critical review. *J Prosthodont Res*. 2018;62(2):121–133. doi:10.1016/j.jpor.2017.07.003
24. Boyan BD, Hummert TW, Dean DD, Schwartz Z. Role of material surfaces in regulating bone and cartilage cell response. *Biomaterials*. 1996;17(2):137–146. doi:10.1016/0142-9612(96)85758-9
25. Zhao Z, Li X, Zou D, Lian Y, Tian S, Dou Z. Expression of microRNA-21 in osteoporotic patients and its involvement in the regulation of osteogenic differentiation. *Exp Ther Med*. 2019;17:709–714. doi:10.3892/etm.2018.6998
26. Yang C, Liu X, Zhao K, Zhu Y, Hu B, Zhou Y, Wang M, Wu Y, Zhang C, Xu J, Ning Y, Zou D. miRNA-21 promotes osteogenesis via the PTEN/PI3K/Akt/HIF-1α pathway and enhances bone regeneration in critical size defects. *Stem Cell Res Ther*. 2019;10(1):65. doi:10.1186/s13287-019-1168-2.
27. Wierzbicka A, Zytkiewicz ZR, Sobańska M, Kłosek K, Łusakowska E. Influence of substrate on crystallographic quality of AlGaN/GaN HEMT structures grown by plasma-assisted MBE. *Acta Phys Pol A*. 2012;121(4):899–902. doi:10.12693/APhysPolA.121.899
28. Colombi P, Zanola P, Bontempi E, Roberti R, Gelfi M, Depero LE. Glancing-incidence X-ray diffraction for depth profiling of polycrystalline layers. *J Appl Crystallogr*. 2006;39(2):176–179. doi:10.1107/S0021889805042779
29. van der Lee A, Roualdes S, Berjoan R, Durand J. Mass density determination of thin organosilicon films by X-ray reflectometry. *Appl Surf Sci*. 2001;173(1–2):115–121. doi:10.1016/S0169-4332(00)00890-4
30. Burnier M, Fricker AF, Hayoz D, Nussberger J, Brunner HR. Pharmacokinetic and pharmacodynamic effects of YM087, a combined V 1 /V 2 vasopressin receptor antagonist in normal subjects. *Eur J Clin Pharmacol*. 1999;55(9):633–637. doi:10.1007/s002280050685
31. Smieszek A, Giezek E, Chrapiec M, et al. The influence of Spirulina platensis filtrates on caco-2 proliferative activity and expression of apoptosis-related microRNAs and mRNA. *Mar Drugs*. 2017;15:3. doi:10.3390/md15030065
32. Marycz K, Weiss C, Śmieszek A, Kornicka K. Evaluation of oxidative stress and mitophagy during adipogenic differentiation of adipose-derived stem cells isolated from Equine Metabolic Syndrome (EMS) Horses Krzysztof. *Stem Cells Int*. 2018;2018:13–15. doi:10.1155/2018/5340756
33. Smieszek A, Czyrek A, Basinska K, et al. Effect of metformin on viability, morphology, and ultrastructure of mouse bone marrow-derived multipotent mesenchymal stromal cells and Balb/3T3 embryonic fibroblast cell line. *Biomed Res Int*. 2015;2015:1–14. doi:10.1155/2015/769402
34. Chomczynski P, Sacchi N. Single-step method of RNA isolation by acid guanidinium thiocyanate-phenol-chloroform extraction. *Anal Biochem*. 1987;162(October2017):156–159. doi:10.1006/abio.1987.9999
35. Smieszek A, Kornicka K, Szłapka-Kosarzewska J, et al. Metformin increases proliferative activity and viability of multipotent stromal stem cells isolated from adipose tissue derived from horses with equine metabolic syndrome. *Cells*. 2019;8:2. doi:10.3390/cells8020080
36. Śmieszek A, Giezek E, Chrapiec M, et al. The Influence of spirulina platensis filtrates on Caco-2 proliferative activity and expression of apoptosis-related microRNAs and mRNA. *Mar Drugs*. 2017;15(3):65. doi:10.3390/md15030065
37. Marycz K, Smieszek A, Trynda J, et al. Nanocrystalline hydroxyapatite loaded with resveratrol in colloidal suspension improves viability, metabolic activity and mitochondrial potential in human adipose-derived mesenchymal stromal stem cells (hASCs). *Polymers (Basel)*. 2019;11:1. doi:10.3390/polym11010092
38. Lis-Bartos A, Smieszek A, Frańczyk K, Marycz K. Fabrication, characterization, and cytotoxicity of thermoplastic polyurethane/poly(lactic acid) material using human adipose derived mesenchymal stromal stem cells (hASCs). *Polymers (Basel)*. 2018;10:10. doi:10.3390/polym10101073
39. Crist B. *Handbooks of Monochromatic XPS Spectra*. XPS International LLC;2005:1.

40. Sygellou L, Gianneta V, Xanthopoulos N, et al. ZrO_2 and Al_2O_3 thin films on Ge(100) grown by ALD: an XPS investigation. *Surf Sci Spectra*. 2011;18(1):58–67. doi:10.1116/11.20100901
41. Pétigny S, Mostéfa-Sba H, Domenichini B, Lesniewska E, Steinbrunn A, Bourgeois S. Superficial defects induced by argon and oxygen bombardments on (110) TiO2 surfaces. *Surf Sci*. 1998;410(2–3):250–257. doi:10.1016/S0039-6028(98)00297-0
42. Morita M, Ohmi T, Hasegawa E, Kawakami M, Ohwada M. Growth of native oxide on a silicon surface. *J Appl Phys*. 1990;68 (3):1272–1281. doi:10.1063/1.347181
43. Morita M, Ohmi T. Characterization and control of native oxide on silicon. *Jpn J Appl Phys*. 1994;33(1):370–374. doi:10.1143/JJAP.33.370
44. Uenuma M, Takahashi K, Sonehara S, et al. Influence of carbon impurities and oxygen vacancies in Al2O3 film on Al2O3/GaN MOS capacitor characteristics. *AIP Adv*. 2018;8:105103. doi:10.1063/1.5041501
45. Kuo D-H, Tzeng K-H, Chien C-H. Characterization of nonstoichiometric TiO2 and ZrO2 thin films stabilized by Al2O3 and SiO2 additions. *J Vac Sci Technol a Vac Surf Film*. 2003;21 (6):1996–2002. doi:10.1116/1.1622675
46. Li H, Wang Z, Fu Q, Zhang J. Plasma miRNA levels correlate with sensitivity to bone mineral density in postmenopausal osteoporosis patients. *Biomarkers*. 2014;19(7):553–556. doi:10.3109/1354750X.2014.935957
47. Ma Y, Shan Z, Ma J, et al. Validation of downregulated microRNAs during osteoclast formation and osteoporosis progression. *Mol Med Rep*. 2016;13(3):2273–2280. doi:10.3892/mmr.2016.4765
48. Zhao W, Dong Y, Wu C, Ma Y, Jin Y, Ji Y. MiR-21 overexpression improves osteoporosis by targeting RECK. *Mol Cell Biochem*. 2015;405(1–2):125–133. doi:10.1007/s11010-015-2404-4
49. Rizzi M, Gatti G, Migliario M, Marchese L, Rocchetti V, Renò F. Effect of zirconium nitride physical vapor deposition coating on preosteoblast cell adhesion and proliferation onto titanium screws. *J Prosthet Dent*. 2014;112(5):1103–1110. doi:10.1016/j.prosdent.2014.04.010
50. Stains JP, Civitelli R. Cell-cell interactions in regulating osteogenesis and osteoblast function. *Birth Defects Res Part C Embryo Today Rev*. 2005;75(1):72–80. doi:10.1002/bdrc.20034
51. Chen Y, Roohani-Esfahani SI, Lu ZF, Zreiqat H, Dunstan CR. Zirconium ions up-regulate the BMP/SMAD signaling pathway and promote the proliferation and differentiation of human osteoblasts. *PLoS One*. 2015;10(1):1–17. doi:10.1371/journal.pone.0113426
52. Lee WC, Guntur AR, Long F, Rosen CJ. Energy metabolism of the osteoblast: implications for osteoporosis. *Endocr Rev*. 2017;38 (3):255–266. doi:10.1210/er.2017-00064
53. Ye M, Shi B. Zirconia nanoparticles-induced toxic effects in osteoblast-like 3T3-E1 cells. *Nanoscale Res Lett*. 2018;13(1):1–2. doi:10.1186/s11671-018-2747-3
54. Fan JB, Liu W, Zhu XH, Cui SY, Cui ZM, Zhao JN. microRNA-7 inhibition protects human osteoblasts from dexamethasone via activation of epidermal growth factor receptor signaling. *Mol Cell Biochem*. 2019;460(1–2):113–121. doi:10.1007/s11010-019-03575-y. Epub 2019 Jul 16
55. Zhang S, Liu Y, Zheng Z, et al. MicroRNA-223 suppresses osteoblast differentiation by inhibiting DHRS3. *Cell Physiol Biochem*. 2018;47 (2):667–679. doi:10.1159/000490021